Research Article | Vol. 30, No. 10 / 9 May 2022 / Optics Express 16145
Optics EXPRESS

Detailed balance analysis of vertical GaAs nanowire array solar cells: exceeding the Shockley Queisser limit

SAJAD HAGHANIFAR[1] AND PAUL W. LEU[1,2,3,*]

[1]Department of Industrial Engineering, University of Pittsburgh, Pittsburgh, PA 15261, USA
[2]Department of Mechanical Engineering, University of Pittsburgh, Pittsburgh, PA 15261, USA
[3]Department of Chemical Engineering, University of Pittsburgh, Pittsburgh, PA 15261, USA
*pleu@pitt.edu

Abstract: We performed detailed balance analysis using rigorous coupled-wave analysis (RCWA) on vertical GaAs nanowire (NW) arrays. Both freestanding NW arrays as well as NW arrays on a perfect back reflector are assessed. Both types of vertical NW arrays demonstrate efficiencies that exceed the Shockley Queisser (SQ) or radiative efficiency limit when the NWs are sufficiently long. The use of a back reflector enhances the efficiency of NW solar cells by increasing solar absorption and suppressing emission from the backside of the solar cell. We study the light trapping and material reduction advantages of NWs. Furthermore, we compare simulations that evaluate detailed balance efficiency with ultimate efficiency and show that ultimate efficiency studies can determine near-optimal solar cells while vastly reducing the number of simulations that need to be performed. While open circuit voltages above the radiative limit can be achieved, tradeoffs with short circuit current must be carefully considered. We also compare our simulation results to other claims in the literature that NWs are capable of exceeding the SQ limit.

1. Introduction

Nanowires (NWs) offer many advantages for solar cells such as low-cost and incorporation into various flexible substrates [1,2]. NWs may be grown epitaxially on substrates with different lattice constants [3,4] or with NWs of other materials [5–7] and may enable multijunctions of mismatched materials as the elastic strain is relaxed in NW geometry. NWs have leaky resonance modes that can be engineered for light trapping and broadband light absorption needed in solar cells [8–13]. GaAs NW array solar cells with 15.3% power conversion efficiency at 1-sun have been demonstrated [14]. Previous simulations of vertical GaAs NW arrays have focused on maximizing the short-circuit current or equivalently, ultimate efficiency [13] without consideration of detailed balance and the open-circuit voltage. Detailed balance analysis has been performed on single horizontal NW solar cells [15], but the analysis performed emphasized open circuit voltage enhancement and performance was only compared with equivalent volume of bulk material. Horizontal NWs are also not scalable to large areas needed for solar cells.

In this work, we performed detailed balance analysis on vertical GaAs NW arrays that are both freestanding and on a perfect back reflector. The transmission, absorption, and reflection of the NW arrays were obtained using rigorous coupled-wave analysis (RCWA). We demonstrate that long vertical NW arrays may exceed the Shockley Queisser (SQ) or radiative efficiency limit. Optimized freestanding NW arrays over 200 μm long exceed the SQ limit. The use of a perfect back reflector improves efficiencies, and these NW efficiencies may exceed the SQ limit when this limit is also calculated with a perfect back reflector. Optimized NW arrays on a perfect back reflector over 100 μm long exceed the SQ limit. We demonstrate the reduction of material possible with NWs by studying the area packing factor and equivalent thicknesses of optimal

#455663 https://doi.org/10.1364/OE.455663
Journal © 2022 Received 9 Feb 2022; revised 11 Apr 2022; accepted 12 Apr 2022; published 27 Apr 2022

Optics EXPRESS

vertical NW arrays. NW arrays with area packing factors under 5% and equivalent thicknesses under 2 μm can absorb over 98% of photons above the GaAs bandgap. The NWs exhibit strong light trapping by enhancing the absorption of light compared to equivalent thickness films. We also compare differences between detailed balance efficiency simulations and ultimate efficiency simulations, which attempt to maximize short circuit current. We demonstrate that ultimate efficiency simulations provide for near-optimal NW solar cells and may provide a way to quickly evaluate different designs as the solar cells only need to be simulated at normal-incidence as opposed to all incidence angles. While open circuit voltages above the radiative limit may be achieved with NWs, tradeoffs with short circuit current must also be considered. We also compare our simulation results with other results that have suggested that NWs are capable of exceeding the SQ limit. Careful consideration of the area of the solar cells as well as assumptions of radiative and non-radiative recombination must be carefully taken into account.

2. Detailed balance analysis

The efficiency of a solar cell is given by

$$\eta = \frac{J(V_m)V_m}{P_s} \tag{1}$$

where V_m is the voltage of the solar cell at its maximum power point and $J(V_m)$ is the the current density at this voltage. P_s is the power density of sunlight which is 1000 W/m^2 for the AM1.5G spectrum [16]. The maximum power point is where the product of the current and voltage is the highest. The current density is defined as

$$J(V) = J_{sc} - J_{rec}(V) \tag{2}$$

where J_{sc} is the short-circuit current density due to absorbed photons and $J_{rec}(V)$ is the thermal recombination current.

The short circuit current density is

$$J_{sc} = J_{max} - J_{rec}(0) \tag{3}$$

where the maximum current density is

$$J_{max} = q\int_0^{\lambda_{bg}} \frac{A(\lambda)I_{AM1.5}(\lambda)}{\hbar 2\pi c/\lambda}d\lambda = q\int_0^{\lambda_{bg}} A(\lambda)b_{AM1.5}(\lambda)d\lambda \tag{4}$$

where $\hbar$ is the reduced Planck constant, c is the speed of light in vacuum, λ is the wavelength of light in vacuum, $I_{AM1.5}(\lambda)$ is the spectral irradiance of the AM1.5G spectrum [16], and $A(\lambda)$ is the absorption of light by the solar cell at normal incidence. $b_{AM1.5}$ is the photon flux density of the AM1.5G spectrum and $b_{AM1.5}(\lambda) = \frac{I_{AM1.5}(\lambda)}{\hbar 2\pi c/\lambda}$. The recombination current is

$$J_{rec}(V) = qf_g F_{c0}\left[\exp\left(\frac{qV}{k_b T}\right) - 1\right] \tag{5}$$

where f_g is a geometric factor and F_{c0} is the density of photons emitted by the solar cell as a blackbody ($V = 0$ and thermal equilibrium) or equivalently, absorbed from the surrounding air treated as a blackbody. $f_g = 2$ when the solar cell is emitting radiation from both the front and rear side and $f_g = 1$ when the solar cell is only emitting radiation from the front side, such as when there is a perfect back reflector. q is the fundamental charge, k_b is Planck's constant, and T is the temperature in Kelvin. We assume the solar cell has a temperature of 289.15 K or 25° C as Shockley and Queisser did in their original paper [17]. The reverse saturation current density

Optics EXPRESS

$J_0 = qf_g F_{c0}$ and Eq. (5) can be written as $J_{rec}(V) = J_0\,[\exp(qV/k_bT) - 1]$. In detailed balance, the absorption is equal to the emission, and thus

$$F_{co} = \int_0^{2\pi}\int_0^{\pi/2}\int_0^{\lambda_g} \Theta(\lambda)\frac{A_{TE}(\lambda,\theta,\phi) + A_{TM}(\lambda,\theta,\phi)}{2}\cos(\theta)\sin(\theta)d\lambda d\theta d\phi \tag{6}$$

where $\Theta(\lambda)$ is the spectral radiance of a blackbody according to Planck's radiation law:

$$\Theta(\lambda) = \frac{c}{\lambda^4}\frac{2}{\exp\left(\frac{\hbar 2\pi c}{\lambda kT}\right) - 1}. \tag{7}$$

$A_{TE}(\lambda,\theta,\phi)$ and $A_{TM}(\lambda,\theta,\phi)$ are the absorptions of the solar cell at a particular wavelength λ, incidence angle θ, and azimuth angle ϕ for TE and TM-polarized light, respectively. λ_g is the wavelength that corresponds to the bandgap of the material. Only radiative recombination is considered; nonradiative recombination such as Auger, Shockley–Read–Hall, and surface recombination are not considered. Solving Eq. (2) for $J(V_{oc}) = 0$, the open circuit voltage is

$$V_{oc} = \frac{k_bT}{q}\ln\left(\frac{J_{sc}}{J_0} + 1\right). \tag{8}$$

The SQ limit or radiative efficiency limit assumes 100% absorption of photons with energy at or above the band gap. Figure 1 plots the SQ limit for emission from both the front and back of the cell ($f_g = 2$; blue) and emission only from the front side of the cell ($f_g = 1$; green). The SQ limit was originally calculated assuming radiation emission from both the front and back of the cell [17]. Under this assumption, the maximum efficiency is 33.16% at a bandgap of $E_g = 1.34$ eV. $V_{oc} = 1.062$, $FF = 0.888$, $J_{sc} = 35.18$ mA/cm^2, and $J_0 = 3.94 \times 10^{-17}$ mA/cm^2. For GaAs, with a bandgap of $E_g = 1.43$ eV, the SQ limit is 32.53% and marked with a blue circle in Fig. 1. $V_{oc} = 1.150$, $FF = 0.895$, and $J_{sc} = 31.64$ mA/cm^2, and $J_0 = 1.16 \times 10^{-18}$ mA/cm^2.

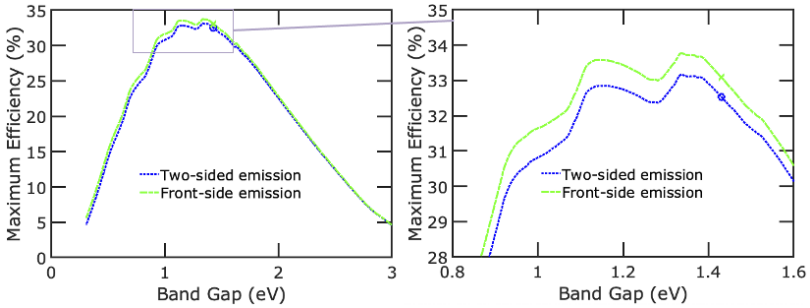

Fig. 1. Shockley Queisser (SQ) limit assuming emission from both the front and back of the material (blue) and only from the front (green). The SQ limit for GaAs with a band gap of 1.43 eV is marked with a blue circle and green x-mark.

We additionally calculate the SQ limit with a perfect back reflector, where the emission is only from the frontside ($f_g = 1$; plotted with green lines). The dark current density J_0 is reduced by a factor of 2 and thus, higher voltages are achievable. In this case, the maximum efficiency is 33.77% at a bandgap of 1.34 eV. $V_{oc} = 1.080$, $FF = 0.889$, $J_{sc} = 35.18$ mA/cm^2, and $J_0 = 1.97 \times 10^{-17}$ mA/cm^2. For GaAs on a back reflector, the SQ limit is higher than without the reflector and 33.09%. $J_{sc} = 31.64$ mA/cm^2, $V_{oc} = 1.173$, $FF = 0.896$, and $J_0 = 5.80 \times 10^{-19}$ mA/cm^2.

Optics EXPRESS

3. Nanowire RCWA simulations

Simulations were performed on the reflection, transmission, and absorption spectra of various vertical NWs using the rigorous coupled-wave analysis (RCWA) method using S4 [18]. Fourier series coefficients were generated by fast Fourier transform (FFT). Figure 2 shows schematics of the two NW systems considered: (a) freestanding NW arrays, and (b) NW arrays on a perfect back reflector. The perfect back reflector was implemented by using a material with the real and imaginary parts of the index of refraction both set to 100, $n = k = 100$ [19]. Perfect back reflectors with various high n and k values were compared (Supplement 1) to show that the solar cell simulation results are not sensitive to the particular choice of high n and k values used.

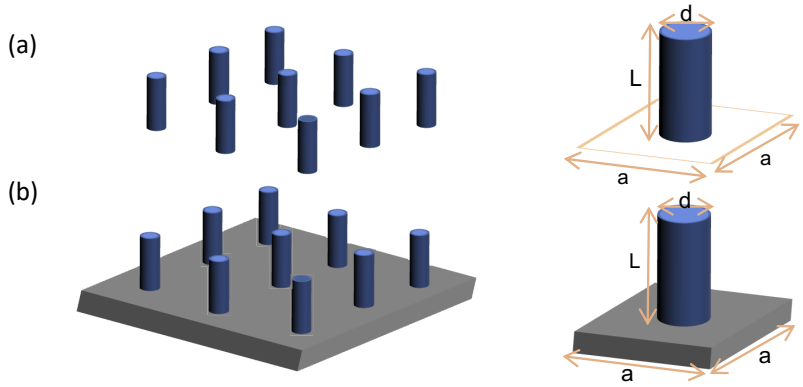

Fig. 2. Schematics of vertical GaAs NW arrays studied. The array (left) and a single unit cell (right) are both shown. (a) Freestanding NW array and (b) NW array on a perfect back reflector. The NW arrays are arranged in a square lattice defined by pitch a, diameter d, and length L.

The corresponding unit cells of a single NW are also shown on the right of Fig. 2. Each NW array system is defined by the NW diameter d, length L, and square array pitch a. The simulations were run over the domains $a \in [50, 1500]$ nm and $d \in [50, 1000]$ nm in 50 nm increments with the constraint $d \leq a$. Quantum confinement effects are ignored as they are only significant for NWs with diameters below about 20 nm [20]. The NW arrays were optimized for maximum efficiency at each length for lengths between 1 and 300 μm. The NW arrays were simulated over all incidence angles and azimuth angles in order to obtain the density of photons emitted by the material as a blackbody F_{co} (Eqn. 6) and the recombination current $J_{rec}(V)$ (Eqn. 5). The maximum current density and short current density were determined by the absorption spectrum at normal incidence.

Figure 3 plots the solar cell properties of the maximum efficiency NW arrays as a function of length for freestanding NW arrays (blue) and NW arrays on a perfect back reflector (green). For each length NW, the maximum efficiency was determined (Fig. 3(a)). The NW arrays have increasing efficiency with increasing length due to increased absorption and higher short circuit current density. The SQ limit for two-sided emission is shown with horizontal blue dotted lines and the SQ limit with only front side emission (or on a perfect back reflector) is shown with horizontal green dash dotted lines.

The maximum efficiency of freestanding NW arrays exceeds the SQ limit at lengths of 200 and 300 μm. At a length of 1 μm, the maximum efficiency is 27.19% and this efficiency increases with longer NWs. The efficiencies of the 200 and 300 μm freestanding NWs are 32.56% and 32.57%, respectively, which is higher than the SQ limit of 32.53%. The use of a perfect back reflector increases the efficiency of the NW arrays as the recombination current density $J_{rec}(V)$ and dark current density J_0 are lowered from the solar cell only emitting from the front side

Optics EXPRESS

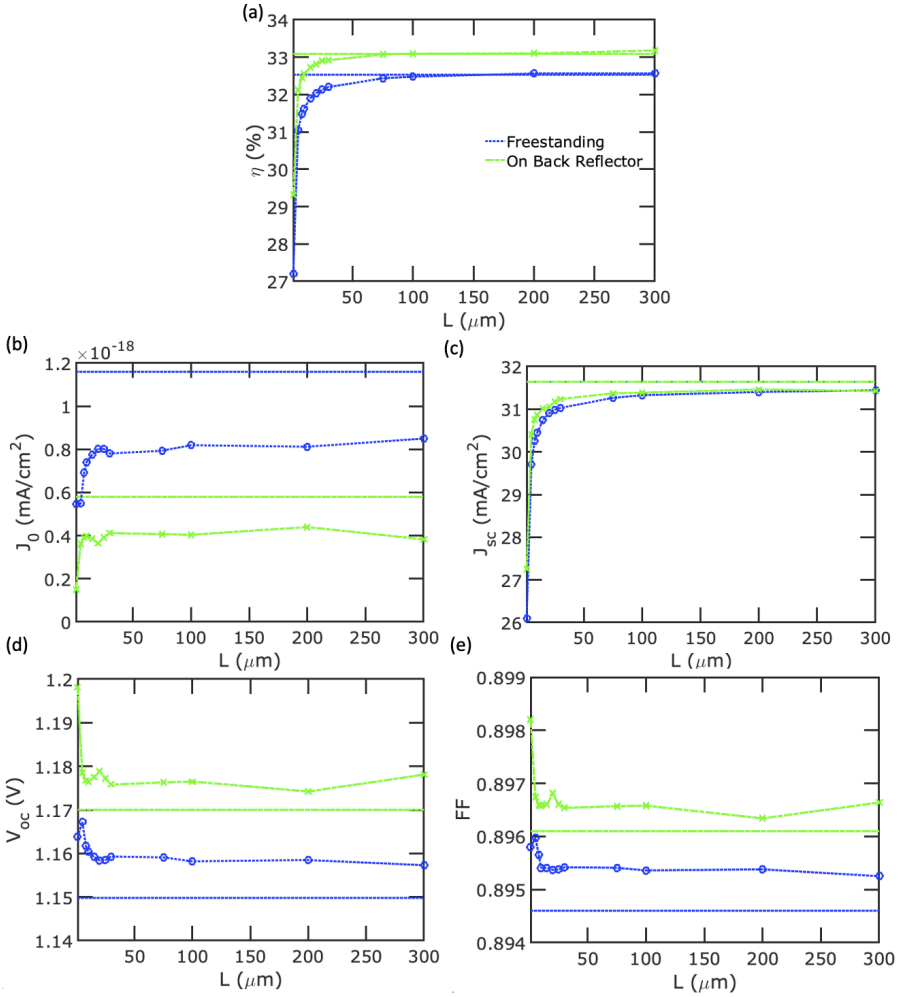

Fig. 3. Optimum efficiency of NW arrays as a function of length. (a) Maximum power conversion efficiency η for freestanding NW arrays (blue) and NW arrays on a perfect back reflector (green). (b) Short circuit current density, (c) reverse saturation current density, (d) open circuit voltage, and (e) fill factor of maximum efficiency NW arrays. The SQ limit for both front and back-sided emission is plotted with horizontal dotted blue lines and for only front-sided emission with dash dotted green lines.

Optics EXPRESS

instead of both the front and back side. The efficiency of the NW arrays on a perfect back reflector is higher than that of freestanding NWs and 29.06% at a length of 1 μm. When the SQ limit is calculated under the same assumption, the SQ limit for bulk GaAs increases to 33.09%. The efficiencies of the 100, 200, and 300 μm long NWs on a perfect back reflector are 33.10, 33.10, and 33.18%, respectively, which exceeds the SQ limit with only frontside emission.

The short circuit current density (Fig. 3(b)), reverse saturation current density (Fig. 3(c)), open circuit voltage (Fig. 3(d)), and fill factor (Fig. 3(e)) are shown for the NW arrays with maximum efficiency. For freestanding NW arrays of 1 μm length, the maximum efficiency NWs have $J_{sc} = 26.10$ mA/cm^2, $J_0 = 5.45 \times 10^{-19}$ mA/cm^2, $V_{oc} = 1.164$ V, and $FF = 0.896$. As the length of the NWs increase, the short circuit current density increases due to increased absorption. For freestanding NW arrays of 300 μm length, the maximum efficiency NWs have $J_{sc} = 31.44$ mA/cm^2, $J_0 = 8.49 \times 10^{-19}$ mA/cm^2, $V_{oc} = 1.157$ V, and $FF = 0.895$. The use of a back reflector increases absorption as light reflected off the back reflector can also be absorbed. NW arrays of 1 μm length on a perfect back reflector with maximum efficiency have $J_{sc} = 27.63$ mA/cm^2, $J_0 = 1.50 \times 10^{-19}$ mA/cm^2, $V_{oc} = 1.174$ V, and $FF = 0.897$. At 300 μm length, the maximum efficiency NW arrays have $J_{sc} = 31.42$ mA/cm^2, $J_0 = 3.83 \times 10^{-19}$ mA/cm^2, $V_{oc} = 1.178$ V, and $FF = 0.897$.

The open circuit voltage depends on the short circuit current density and the reverse saturation current density (Eq. (8)). While the NW arrays have lower short circuit current density than the SQ limit, they also have lower reverse saturation current density. This allows for open circuit voltages and fill factors above that of the SQ limit. Adding a back reflector to the NW arrays decreases the reverse saturation current density from the freestanding NWs, and thus increases the open circuit voltage and fill factor. Open circuit voltage enhancement above that of bulk GaAs (the radiative limit) is related to suppressing the photons emitted by the cell in the spectral vicinity above the band gap [15] as these photons contribute most strongly to the reverse saturation current. Our simulations indicate that open circuit voltage enhancements above the radiative limit are possible with NW solar cells as has been previously demonstrated [15,21].

Figure 4 plots the geometry of the optimum NW arrays as a function of length. The diameter (left y-axis) and pitch (right y-axis) of the optimum NW arrays are shown (Fig. 4(a)) for NWs that are (i) freestanding and (ii) on a perfect back reflector. In the case of 1 μm long freestanding NWs, diameter $d = 350$ nm and pitch $a = 550$ nm provides the best efficiency. For longer freestanding NWs of length 5 μm and longer, the optimum diameter is 150 nm, while optimum pitch size increases with the length of NW. The optimum NW array on back reflector has a diameter of 150 nm for all lengths, except 100 nm at a length of 300 μm while the pitch increases with increasing length.

Figure 4(b)(i) shows the area packing factor of the NW arrays, $APF = \pi d^2/(4a^2)$ and (ii) the equivalent thickness of the NW arrays $L_{eq} = APF \times L$. Optimum freestanding NWs have an area packing factor of 0.318 at 1 μm length that decreases to 0.012 at 300 μm length. The optimal NWs on a perfect back reflector have an area packing factor of 0.144 at 1 μm length that decreases to 0.003 at 300 μm length. Due to the low area packing factor of these NWs, the equivalent thicknesses of optimal NWs are all under 4 μm (Fig. 4(bii)). The thickness of a typical GaAs thin film solar cell is about 4 μm [22].

Figure 5 shows results on the 20 μm long optimized NW arrays. The freestanding NW array is defined by $d = 150$ nm and $a = 650$ nm, while the NW array on perfect back reflector is defined by $d = 150$ nm and $a = 850$ nm. The freestanding NWs have $\eta = 32.04\%$, $J_{sc} = 30.90$ mA/cm^2, $V_{oc} = 1.158$, and $FF = 0.895$. The NWs on back reflector have $\eta = 32.82\%$, $J_{sc} = 31.05$ mA/cm^2, $V_{oc} = 1.179$, and $FF = 0.897$. Figure 5(a) plots the absorption (or emission) spectra of these NWs as a function of photon energy (radial direction) and incidence angle θ (polar direction) for (i) freestanding NWs and (ii) NWs on a perfect back reflector. The absorption shown is averaged all possible injection azimuth angles ϕ. The absorption of freestanding NWs are symmetric for

Optics EXPRESS

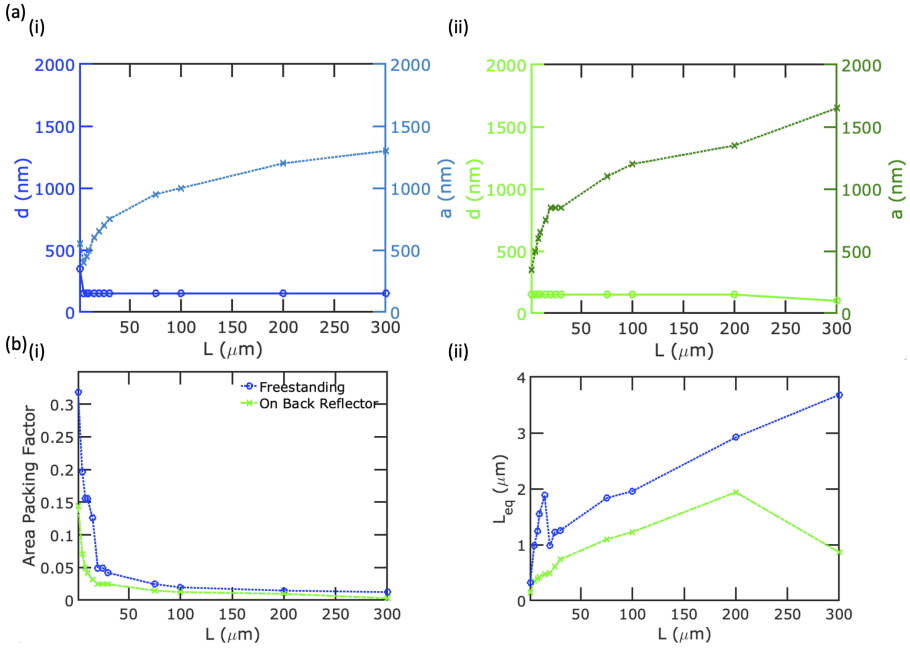

Fig. 4. Geometry of maximum efficiency NW arrays as a function of length. (a) Diameter (right y-axis) and pitch (left y-axis) of maximum efficiency NW arrays that are (i) freestanding and (ii) on a perfect back reflector. (b)(i) Area fill factor and (ii) equivalent thickness of optimal NW arrays.

positive and negative incidence angles as well as from the front and the back. The absorption of NWs on a perfect back reflector is symmetric for positive and negative incidence angles, but there is no absorption from the backside. Figure 5(b) plots the AM1.5G solar integrated absorption of the NWs,

$$A_{sol} = \frac{\int_0^{\lambda_g} A(\lambda, \theta = 0, \phi = 0) b_{AM1.5}(\lambda) d\lambda}{\int_0^{\lambda_g} b_{AM1.5}(\lambda) d\lambda}. \tag{9}$$

The solar absorption shown is the fraction of photons above the bandgap of GaAs that are absorbed. The solar absorption is 97.66% at normal incidence for the freestanding NW array, while it is 98.13% at normal incidence for the NW array on a perfect back reflector. The absorption is very broad angle where even at high incidence angles remains very high. At $\theta = 70°$, the freestanding NW array has a solar absorption of 86.69%, while the NW on a perfect back reflector has a solar absorption of 90.00%.

Using the equivalent thickness as a fitting parameter, we find that the freestanding thin film would need to be about 2.0 μm thick to absorb as much light as the freestanding vertical GaAs NW array. A thin film on a perfect back reflector would need to be about 1.1 μm thick to absorb as much light as the vertical GaAs NWs on perfect back reflector. This demonstrates the light trapping effect in the vertical NWs where the freestanding NWs are able to absorb as much light as films with 2.4 × more material; NWs on a perfect back reflector are able to absorb as much light as films with 2.2 × more material. Table 1 summarizes the results on the 20 μm long NWs in comparison to bulk GaAs and equivalent thickness thin films.

Figure 6 shows results on the 200 μm long optimized NW arrays. The freestanding NW array is defined by $d = 150$ nm and $a = 1350$ nm, while the NW array on perfect back reflector is defined by $d = 150$ nm and $a = 1200$ nm. The freestanding NWs have $\eta = 32.56\%$, $J_{sc} = 31.40$ mA/cm^2,

Optics EXPRESS

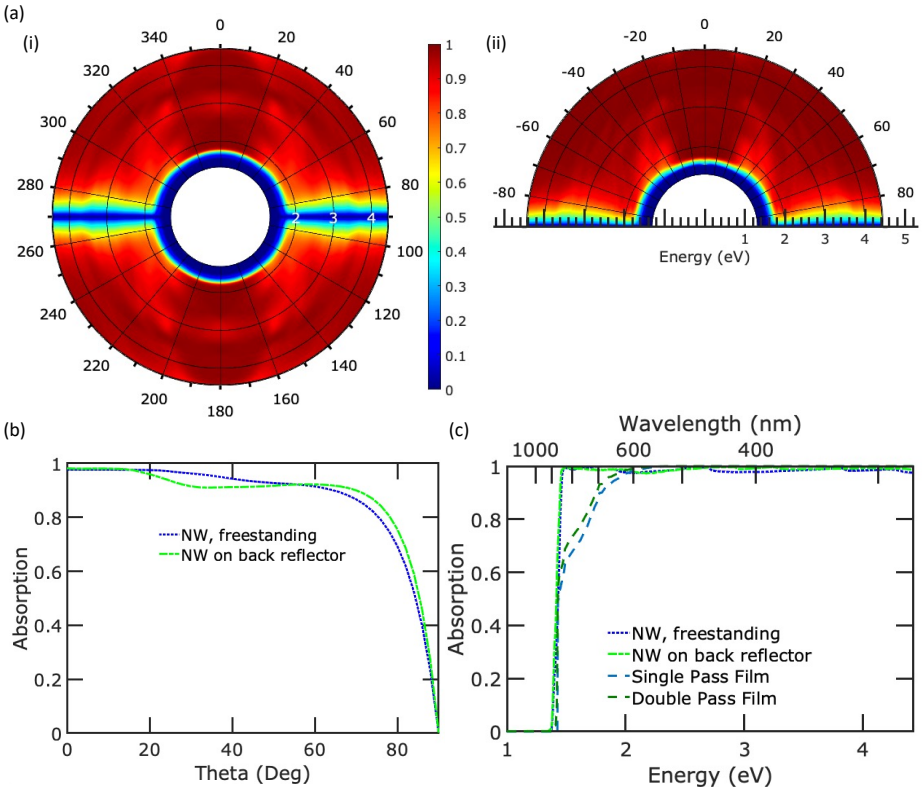

Fig. 5. Absorption spectra of optimal 20 μm length NWs. Absorption as a function of photon energy (radial direction) and incidence angle θ (polar direction) for (i) freestanding NWs and (ii) NWs on a perfect back reflector. (b) Solar integrated absorption as a function of incidence angle. (c) Absorption spectra at $\theta = 0$.

Table 1. GaAs solar cell comparison with 20 μm long NWs and equivalent thickness thin films.

Solar Cell	η (%)	A_{sol} (%)	J_{sc} (mA/cm^2)	V_{oc} (V)	FF	J_0 (mA/cm^2)
Bulk	32.53	100.00	31.64	1.150	0.895	1.16×10^{-18}
Bulk on PBR	33.09	100.00	31.64	1.173	0.896	5.80×10^{-19}
20 μm NW	32.04	97.66	30.90	1.158	0.895	8.03×10^{-19}
20 μm NW on PBR	32.82	98.13	31.05	1.179	0.897	3.65×10^{-19}
Equivalent Thickness	28.55	88.02	27.85	1.146	0.895	1.16×10^{-18}
Equivalent Thickness on PBR	29.84	90.44	28.62	1.165	0.896	5.80×10^{-19}

Optics EXPRESS

V_{oc} = 1.158, and FF = 0.895. The NWs on back reflector have η = 33.10%, J_{sc} = 31.46 mA/cm^2, V_{oc} = 1.174, and FF = 0.896. Figure 6(a) plots the absorption (or emission) spectra of these NWs as a function of photon energy (radial direction) and incidence angle θ (polar direction) for (i) freestanding NWs and (ii) NWs on a perfect back reflector. The solar absorption is 98.01% at normal incidence for the freestanding NW array, while it is 99.44% at normal incidence for the NW array on a perfect back reflector. The absorption is again very broad angle. At θ = 70°, the freestanding NW array has a solar absorption of 94.38%, while the NW on a perfect back reflector has a solar absorption of 96.08%.

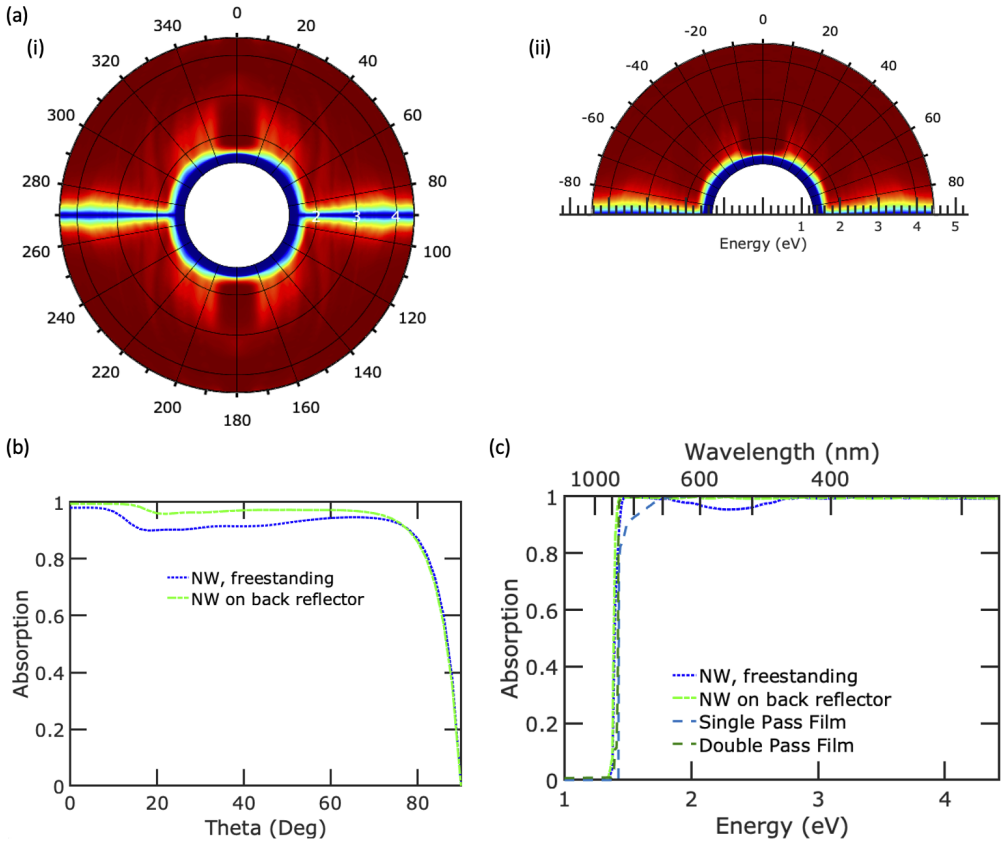

Fig. 6. Absorption spectra of optimal 200 μm length NWs. Absorption as a function of photon energy (radial direction) and incidence angle θ (polar direction) for (i) freestanding NWs and (ii) NWs on a perfect back reflector. (b) Solar integrated absorption as a function of incidence angle. (c) Absorption spectra at θ = 0.

Figure 6(c) shows the absorption spectra of freestanding NWs and NWs on perfect back reflector at normal incidence. As can be seen, the absorption spectra are nearly step functions, thus resulting in solar absorptions that are almost equal to 1. For comparison, we also plot the absorption of GaAs thin films with the same equivalent thickness of material as the NWs. The freestanding thin film is about 2.5 μm in thickness, while the thin film on back reflector is 1.9 μm in thickness. The solar absorption is 97.49% and 99.95% for these two thin films, respectively. While shorter NWs have strong light trapping effect to enhance the light absorption and short circuit current compared to equivalent thickness films [13], the 200 μm long NWs do not exhibit such an effect due to their long lengths. Table 2 summarizes the results on the 200 μm long NWs

Optics EXPRESS

in comparison to bulk GaAs and equivalent thickness thin films. NWs at these lengths exceed the SQ limit.

Table 2. GaAs solar cell comparison with 200 μm long NWs and equivalent thickness thin films.

Solar Cell	η (%)	A_{sol} (%)	J_{sc} (mA/cm^2)	V_{oc} (V)	FF	J_0 (mA/cm^2)
200 μm NW	32.56	98.01	31.40	1.158	0.895	8.12×10^{-19}
200 μm NW on PBR	33.10	99.44	31.46	1.174	0.896	4.39×10^{-19}
Equivalent Thickness	32.23	97.49	30.85	1.167	0.896	1.16×10^{-18}
Equivalent Thickness on PBR	32.52	99.95	31.63	1.150	0.895	5.80×10^{-19}

Figure 7 shows contour plots of the photovoltaic characteristics of 200 μm NW arrays that are (a) freestanding and (b) on a perfect back reflector as a function of diameter and pitch. The (i) efficiency, (ii) short circuit current density, (iii) open circuit voltage, and (iv) fill factor of the NW arrays are shown. The NW array with maximum efficiency, short circuit current density, and open circuit voltage are marked with a circle and plus, respectively. Small diameter NWs below 100 nm tend to have weak solar absorption. Larger diameter NWs where the diameter is close to the pitch also result in lower absorption as the reflection is increased [13,23].

The NW solar cell with maximum short circuit current density is marked in Fig. 7 with a plus for comparison purposes. Many simulation studies on NWs and other nanostructures have focused on evaluating their ultimate efficiency [13,23–26], where maximizing the ultimate efficiency is equivalent to maximizing the short circuit current density. The ultimate efficiency is less computationally expensive to simulate as the solar cell only needs to be simulated at normal incidence as opposed to all incidence angles in the detailed balance case. The ultimate efficiency is calculated by assuming that each photon absorbed produces one electron-hole pair and these carriers are collected without recombination such as when the temperature of the cell is 0 K. These calculations typically use room-temperature bandgap and n and k values, so the efficiency analysis is theoretically inconsistent. In these simulations, $J_{rec}(V) = 0$ and $V_{oc} = E_g/q$, and thus, maximizing the ultimate efficiency is equivalent to maximizing the short circuit current density.

The 200 μm long freestanding NW arrays with maximum short circuit current density (or ultimate efficiency) have a diameter of 150 nm and a pitch of 1200 nm. These NWs have $\eta = 32.54\%$, $J_{sc} = 31.46$ mA/cm^2, $V_{oc} = 1.156$, and $FF = 0.895$. The efficiency of these NWs is slightly smaller than those that have been optimized for maximum efficiency, which have $\eta = 32.57\%$, $J_{sc} = 31.44$ mA/cm^2, $V_{oc} = 1.157$ V, and $FF = 0.895$. On a back reflector, the maximum short circuit current density (or ultimate efficiency) NW arrays have a diameter of 100 nm and pitch of 1550 nm. For these NWs, $\eta = 33.17\%$, $J_{sc} = 31.44$ mA/cm^2, $V_{oc} = 1.177$ V, and $FF = 0.897$. In comparison, NWs that have been optimized for efficiency have $\eta = 33.18\%$, $J_{sc} = 31.42$ mA/cm^2, $V_{oc} = 1.178$ V and $FF = 0.897$.

Some simulation studies on NW solar cells have focused on maximizing their open circuit voltage. For example, Korzun et. al. demonstrated that a single NW solar cell may be designed to operate at an open circuit voltage of 0.159 V over the radiative limit by tapering the nanowire and using a plano-convex microlens [21]. This paper prioritizes optimization of open circuit voltage on the rationale that the optimization of short circuit current or similarly, absorption of photons with energy above the band gap, is already near that of radiative limit. However, this study focuses on optimization of open circuit voltage without considering its effect on short circuit current and overall efficiency. Our results (Fig. 7) indicate that there are strong tradeoffs between current and voltage, where NW arrays with higher current density tend to have lower voltage and vice versa.

The 200 μm long freestanding NWs with maximum open circuit voltage have a diameter of 50 nm and pitch of 1500 nm. These optimized NWs have $\eta = 28.86\%$, $J_{sc} = 27.28$ mA/cm^2,

Optics EXPRESS

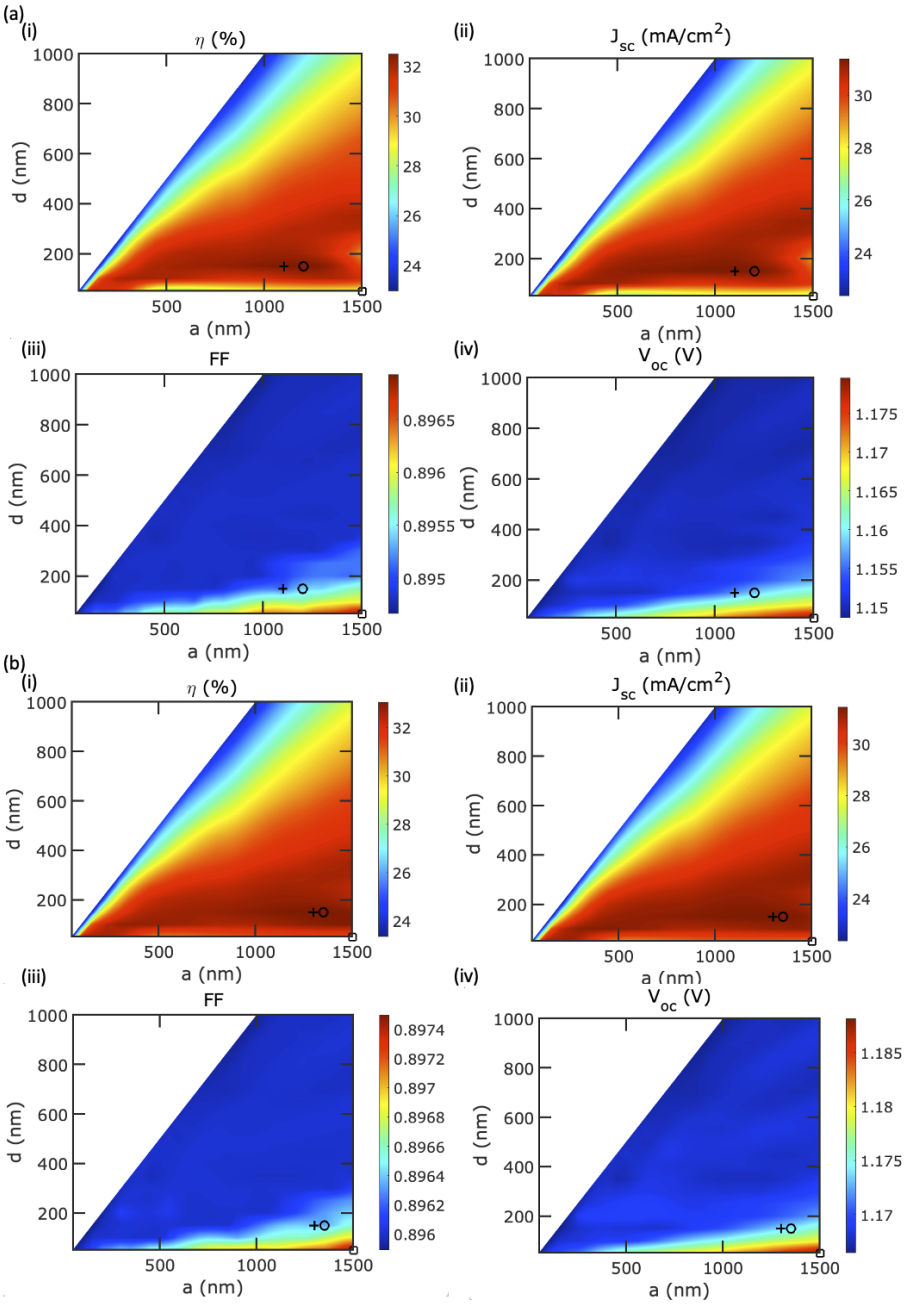

Fig. 7. Solar module performance as a function of pitch a and diameter d for NW arrays of length $L = 200$ μm for (a) freestanding NW array and (b) NW array on perfect back reflector. (i) η, (ii) J_{sc}, (iii) V_{oc} and (iv) FF. The NW array with maximum η, J_{sc}, and V_{oc} are marked with a circle, plus, and square, respectively.

Optics EXPRESS

V_{oc} = 1.180 V, and FF = 0.897. This open circuit voltage represents a 0.030 V enhancement over the radiative limit of V_{oc} = 1.150 V. However, the efficiency of these NWs is substantially lower than those that have been optimized for efficiency (32.56%). On a perfect back reflector, the maximum open circuit NW arrays also have a diameter of 50 nm and pitch of 1500 nm. For these NWs, η = 31.30%, J_{sc} = 29.37 mA/cm^2, V_{oc} = 1.188 V, and FF = 0.898. This open circuit voltage represents a 0.018 V enhancement over the radiative limit of V_{oc} = 1.170 V. However, like the freestanding NWs, the efficiency of these NWs is much lower than those that have been optimized for efficiency (33.10%). It should be noted that our optimum open circuit voltage NW arrays are at the corner of the simulation domain. Further open circuit voltage optimization could be achieved through NW arrays with smaller diameters and larger pitches. However, our results suggest that there is limited utility to open circuit voltage optimization alone without consideration of tradeoffs with short circuit current. NWs with optimized open circuit voltages have substantially lower short circuit currents and efficiencies than NW arrays that have been optimized for only efficiency.

Figure 8 compares the efficiency of NW arrays that have been optimized for maximum power conversion efficiency, maximum short circuit current density, and maximum open circuit voltage across all the lengths simulated. NW arrays that have been optimized for open circuit voltages can demonstrate voltages above the radiative limit, but tend to have poor short circuit currents and much lower power conversion efficiencies. Open circuit voltage optimization also offers no benefits in terms of computational speed as detailed balance simulations are needed. In contrast, the maximum short circuit current density NWs have almost the same efficiency as those that have been maximized for efficiency. Optimization of short circuit current density (or equivalently, ultimate efficiency) only requires simulations at normal incidence and thus, may save computational time. Thus, they may be useful for quickly determining NWs or other nanostructured solar cells that are near-optimal. It should also be noted that while the NWs that have been optimized for short circuit current have slightly lower efficiencies than those that have been optimized for efficiency, they are still nevertheless able to exceed the SQ limit.

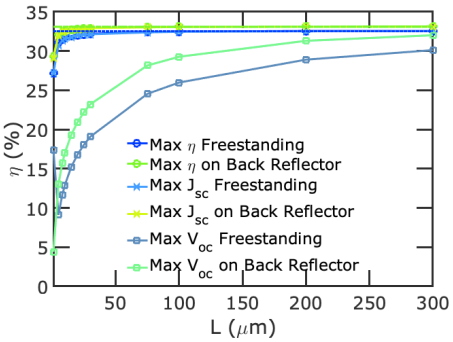

Fig. 8. Efficiency comparison between NWs that have been optimized for maximum efficiency (circles), maximum short circuit current (pluses), and maximum open circuit voltage (squares).

Measurements of single NW solar cells have proclaimed power conversion efficiencies over the SQ limit [27]. However, these measurements only used the cross-sectional area of the single NW in determining the power conversion efficiency, and this analysis does not scale with area. It is well-known that sub-wavelength NWs collect light from larger areas than only their cross-section. For example, our optimized vertical NW arrays over 20 μm long have an area packing factor of less than 5%. However, the area in between the NWs is also included in our efficiency analysis. While the vertical NW arrays may enable large reductions of material, careful consideration of the areas must also be considered in determining whether NWs exceed the SQ limit.

Optics EXPRESS

Another paper determined that vertical InP NWs on a substrate with index of refraction $n = 3.5$ have an efficiency that approaches 32.5% [28]. However, the SQ limit used in this paper is not strictly radiative-recombination limited as it assumes a semi-infinite inactive bulk substrate. An inactive substrate must have non-radiative recombination as its photon absorption/emission rate does not equal that of the surrounding ambient air. With a bulk inactive substrate assumption, the SQ limit is 31.0% at the InP band gap of 1.34 eV. In contrast, under the assumption of only radiative recombination and no back reflector, the SQ limit or radiative efficiency limit for a material with a bandgap of 1.34 eV should have an efficiency of 33.16% (Fig. 1 and [29]).

Vertical GaAs NW array solar cells have also been simulated and provided as an example of a nanostructured solar cell that could exceed the SQ limit [30]. However, in this study, the efficiencies of the NW solar cells are only compared with that of a bulk 80 μm thick GaAs solar cell with double-layer antireflection coating. The 80 μm thick GaAs solar cell has an efficiency of 28.09%, which is much lower than the SQ limit of GaAs without a perfect back reflector (32.53%). The open circuit voltage enhancement of NW array solar cells over the radiative limit is also noted in this paper, but at the expense of a large decrease in light generated current. While such open circuit voltage enhancements have been highlighted in other literature [15,21], there are tradeoffs between voltage and current (Fig. 7) and both need to be carefully considered for how they affect efficiency.

4. Conclusion

In conclusion, we performed detailed balance analysis with rigorous coupled-wave analysis (RCWA) for vertical GaAs NW arrays with and without back reflector. We showed that adding a back reflector enhances the detailed balance efficiency of the GaAs NW array solar cell. The efficiencies of both freestanding vertical GaAs NWs as well as vertical GaAs NWs on a perfect back reflector may exceed the SQ limit. We studied the effect of design parameters on photovoltaic characteristics of GaAs NW array solar cells and demonstrate the light trapping and absorption enhancement of vertical NWs. Furthermore, we show that ultimate efficiency simulations, which only require simulations at normal incidence, may be utilized to obtain near-optimal solar cell designs for detailed balance efficiency. Open circuit optimization, in contrast, results in poor short circuit currents and low efficiencies. Finally, we comment on some other reports in the literature claiming that NWs may exceed the SQ limit. Careful consideration of the area of the solar cells as well as assumptions of radiative and non-radiative recombination must be carefully taken into account.

Funding. National Science Foundation (1552712, 1930582).

Acknowledgments. This research was supported in part by National Science Foundation (NSF) (1552712 and 1930582). This research was supported in part by the University of Pittsburgh Center for Research Computing through the resources provided. The authors thank Dr. Nicklas Anttu for helpful discussions.

Disclosures. The authors declare no conflicts of interest.

Data availability. Data underlying the results presented in this paper are not publicly available at this time but may be obtained from the authors upon reasonable request.

Supplemental document. See Supplement 1 for supporting content.

References

1. Z. Fan, D. J. Ruebusch, A. a. Rathore, R. Kapadia, O. Ergen, P. W. Leu, and A. Javey, "Challenges and prospects of nanopillar-based solar cells," Nano Res. **2**(11), 829–843 (2009).
2. S. Haghanifar, A. J. Galante, and P. W. Leu, "Challenges and Prospects of Bio-Inspired and Multifunctional Transparent Substrates and Barrier Layers for Optoelectronics," ACS Nano **14**(12), 16241–16265 (2020). Publisher: American Chemical Society.
3. P. W. Leu, H. Adhikari, M. Koto, K. Kim, P. D. Rouffignac, A. F. Marshall, R. G. Gordon, C. E. D. Chidsey, and P. C. Mcintyre, "Oxide-encapsulated vertical germanium nanowire structures and their DC transport properties," Nanotechnology **19**(48), 485705 (2008).

Optics EXPRESS

4. S. Hu, P. W. Leu, A. F. Marshall, and P. C. Mcintyre, "Single-crystal germanium layers grown on silicon by nanowire seeding," Nat. Nanotechnol. **4**(10), 649–653 (2009).
5. T. J. Kempa, B. Tian, D. R. Kim, J. Hu, X. Zheng, and C. M. Lieber, "Single and tandem axial p-i-n nanowire photovoltaic devices," Nano Lett. **8**(10), 3456–3460 (2008).
6. L. C. Chuang, M. Moewe, C. Chase, N. P. Kobayashi, C. Chang-Hasnain, and S. Crankshaw, "Critical diameter for III-V nanowires grown on lattice-mismatched substrates," Appl. Phys. Lett. **90**(4), 043115 (2007).
7. F. Glas, "Critical dimensions for the plastic relaxation of strained axial heterostructures in free-standing nanowires," Phys. Rev. B **74**(12), 121302 (2006).
8. L. Tsakalakos, J. Balch, J. Fronheiser, M. Shih, S. F. LeBoeuf, M. Pietrzykowski, P. J. Codella, B. A. Korevaar, O. V. Sulima, J. Rand, A. Davuluru, and U. Rapol, "Strong broadband optical absorption in silicon nanowire films," J. Nanophotonics **1**(1), 013552 (2007).
9. J. Zhu, Z. Yu, G. F. Burkhard, C. Hsu, S. T. Connor, Y. Xu, Q. Wang, M. McGehee, S. Fan, and Y. Cui, "Optical absorption enhancement in amorphous silicon nanowire and nanocone arrays," Nano Lett. **9**(1), 279–282 (2009).
10. G. Mariani, P.-S. Wong, A. M. Katzenmeyer, F. Léonard, J. Shapiro, and D. L. Huffaker, "Patterned Radial GaAs Nanopillar Solar Cells," Nano Lett. **11**(6), 2490–2494 (2011).
11. O. L. Muskens, J. G. Rivas, R. E. Algra, E. P. A. M. Bakkers, and A. Lagendijk, "Design of light scattering in nanowire materials for photovoltaic applications," Nano Lett. **8**(9), 2638–2642 (2008).
12. B. Wang and P. W. Leu, "Tunable and selective resonant absorption in vertical nanowires," Opt. Lett. **37**(18), 3756–3758 (2012).
13. B. Wang, E. Stevens, and P. W. Leu, "Strong broadband absorption in GaAs nanocone and nanowire arrays for solar cells," Opt. Express **22**(S2), A386–A395 (2014).
14. I. Åberg, G. Vescovi, D. Asoli, U. Naseem, J. P. Gilboy, C. Sundvall, A. Dahlgren, K. E. Svensson, N. Anttu, M. T. Björk, and L. Samuelson, "A GaAs Nanowire Array Solar Cell With 15.3% Efficiency at 1 Sun," IEEE J. Photovoltaics **6**(1), 185–190 (2016). Conference Name: IEEE Journal of Photovoltaics.
15. S. Sandhu, Z. Yu, and S. Fan, "Detailed Balance Analysis and Enhancement of Open-Circuit Voltage in Single-Nanowire Solar Cells," Nano Lett. **14**(2), 1011–1015 (2014).
16. "Reference Air Mass 1.5 Spectra," (2020).
17. W. Shockley and H. J. Queisser, "Detailed balance limit of efficiency of p-n junction solar cells," J. Appl. Phys. **32**(3), 510–519 (1961).
18. V. Liu and S. Fan, "S^4 : A free electromagnetic solver for layered periodic structures," Comput. Phys. Commun. **183**(10), 2233–2244 (2012).
19. M. Peters, M. Rüdiger, B. Bläsi, and W. Platzer, "Electro – optical simulation of diffraction in solar cells," Opt. Express **18**(S4), A584–A593 (2010). Publisher: Optical Society of America.
20. G. Zhang, K. Tateno, H. Sanada, T. Tawara, H. Gotoh, and H. Nakano, "Synthesis of GaAs nanowires with very small diameters and their optical properties with the radial quantum-confinement effect," Appl. Phys. Lett. **95**(12), 123104 (2009). Publisher: American Institute of Physics.
21. K. Korzun, G. W. Castellanos, D. K. G. de Boer, J. Gómez Rivas, and J. E. M. Haverkort, "Nanowire solar cell above the radiative limit," Adv. Opt. Mater. **9**(2), 2001636 (2021).
22. G. J. Bauhuis, J. J. Schermer, P. Mulder, M. M. A. J. Voncken, and P. K. Larsen, "Thin film GaAs solar cells with increased quantum efficiency due to light reflection," Sol. Energy Mater. Sol. Cells **83**(1), 81–90 (2004).
23. B. Wang and P. W. Leu, "Enhanced absorption in silicon nanocone arrays for photovoltaics," Nanotechnology **23**(19), 194003 (2012).
24. B. Wang, K. P. Chen, and P. W. Leu, "Engineering inverse woodpile and woodpile photonic crystal solar cells for light trapping," Nanotechnology **27**(22), 225404 (2016).
25. T. Gao, B. Wang, and P. W. Leu, "Plasmonic nanomesh sandwiches for ultrathin film silicon solar cells," J. Opt. **19**(2), 025901 (2017).
26. C. Lin and M. L. Povinelli, "Optical absorption enhancement in silicon nanowire arrays with a large lattice constant for photovoltaic applications," Opt. Express **17**(22), 19371–19381 (2009).
27. P. Krogstrup, H. I. Jørgensen, M. Heiss, O. Demichel, J. V. Holm, M. Aagesen, J. Nygard, and A. Fontcuberta i Morral, "Single-nanowire solar cells beyond the Shockley–Queisser limit," Nat. Photonics **7**(4), 306–310 (2013).
28. N. Anttu, "Shockley–queisser Detailed Balance Efficiency Limit for Nanowire Solar Cells," ACS Photonics **2**(3), 446–453 (2015).
29. S. Rühle, "Tabulated values of the Shockley–Queisser limit for single junction solar cells," Sol. Energy **130**, 139–147 (2016).
30. Y. Xu, T. Gong, and J. N. Munday, "The generalized shockley-queisser limit for nanostructured solar cells," Sci. Rep. **5**(1), 13536 (2015).